Smart Structures and Systems, *Vol. 25, No. 2 (2020) 241-254*
DOI: https://doi.org/10.12989/sss.2020.25.2.241

Seismic vibration control of an innovative self-centering damper using confined SMA core

Canxing Qiu*[1], Zhaohui Gong[2b], Changle Peng[2c] and Han Li[2d]

[1] *Key Laboratory of Urban Security and Disaster Engineering of Ministry of Education, Beijing University of Technology, Beijing 100124, China*
[2] *School of Civil Engineering, Shandong University, Jinan, 250061, China*

(*Received April 1, 2019, Revised June 27, 2019, Accepted August 15, 2019*)

Abstract. Using confined shape memory alloy (SMA) bar or plate, this study proposes an innovative self-centering damper. The damper is essentially properly machined SMA core, i.e., bar or plate, that encased in buckling-restrained device. To prove the design concept, cyclic loading tests were carried out. According to the test results, the damper exhibited desired flag-shape hysteretic behaviors upon both tension and compression actions, although asymmetric behavior is noted. Based on the experimental data, the hysteretic parameters that interested by seismic applications, such as the strength, stiffness, equivalent damping ratio and recentering capacity, are quantified. Processed in the Matlab/Simulink environment, a preliminary evaluation of the seismic control effect for this damper was conducted. The proposed damper was placed at the first story of a multi-story frame and then the original and controlled structures were subjected to earthquake excitations. The numerical outcome indicated the damper is effective in controlling seismic deformation demands. Besides, a companion SMA damper which represents a popular type in previous studies is also introduced in the analysis to further reveal the seismic control characteristics of the newly proposed damper. In current case, it was found that although the current SMA damper shows asymmetric tension-compression behavior, it successfully contributes comparable seismic control effect as those having symmetrical cyclic behavior. Additionally, the proposed damper even shows better global performance in controlling acceleration demands. Thus, this paper reduces the concern of using SMA dampers with asymmetric cyclic behavior to a certain degree.

Keywords: shape memory alloy; experimental test; seismic analysis; vibration control

1. Introduction

Through performing hysteretic behavior, seismic dampers absorb input earthquake energy to protect the main structures from being damaged. This seismic design of using additional dampers has been well recognized for decades, and a variety of dampers have been invented and implemented in practice (Soong and Dargush 1997). Passive dampers are usually more favorable than the other types in seismic protection projects, due to stable hysteresis, low cost and convenient maintenance. Representatives primarily include metallic dampers (Whittaker *et al*. 1991, Tsai *et al*. 1993, Bartera and Giacchetti 2004), viscoelastic dampers (Samali and Kwok 1995, Min *et al*. 2004) and friction dampers (Colajanni and Papia 1995, Mualla and Belev 2002, Bhaskararao and Jangid 2006). However, related studies (Sabelli *et al*. 2003, Fahnestock *et al*. 2007, Tremblay *et al*. 2008, Zhu and Zhang 2007, Qiu and Zhu 2016, Tian and Qiu 2018) indicated that conventional dampers are confident in reducing the peak seismic demands for structures, but their capacity of controlling residual deformation is not that satisfactory. As a result, the protected structures are still at risk of suffering from excessive residual deformation, which leads to challengeable and costly repairing work and even final demolishment.Therefore, increasing awareness is being paid on the effort of reducing post-earthquake residual deformations.

In past years, the community found using shape memory alloy (SMA) is a potential resort to the problem. In earthquake engineering, the most favorite SMA is the superelastic Ni-Ti SMA, due to the combined merits of excellent recentering ability, high fatigue life, good corrosion resistant and high damper and price advantage (DesRoches and Smith 2004, Song *et al*. 2006, Casciati and Marzi 2011, Liu *et al*. 2011, Carreras *et al*. 2011, Casciati *et al*. 2017, Katariya *et al*. 2017). A schematic view of the cyclic behavior of Ni-Ti SMA at temperature above austenite finish transformation threshold (A_f) is shown in Fig. 1. The applied stress triggers the start of phase transformation, and the transformation process forms a plateau until the finish of phase transformation. The reversible loading and unloading paths enclose a practically rhombus area, implying a damping mechanism. In particular, the Ni-Ti alloy can immediately recover deformed shape up to 6%~8% strain when the applied stress is removed (DesRoches *et al*. 2004, Qiu and Zhu 2014). In the early stage, SMA wires are often the key elements of

*Corresponding author, Professor,
E-mail: qiucanxing@bjut.edu.cn
[a] Ph.D., E-mail: qiucanxing@bjut.edu.cn
[b] M.S. Student, E-mail: 13717589869@163.com
[c] M.S. Student, E-mail: 958503343@qq.com
[d] M.S. Student, E-mail: lihan_z@sdu.edu.cn

ISSN: 1738-1584 (Print), 1738-1991 (Online)

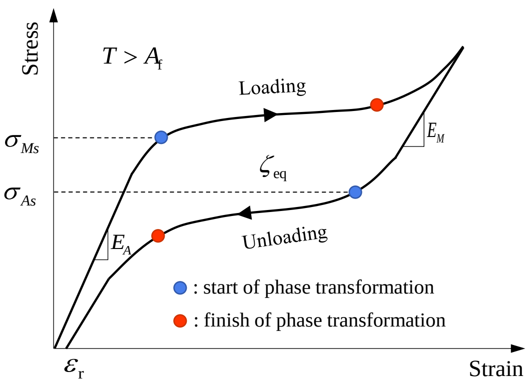

Fig. 1 Schematic of the hysteresis of superelastic Ni-Ti SMA

these damping devices (Dolce *et al*. 2000, Zhang and Zhu 2008, Torra *et al*. 2014, Qiu and Zhu 2017a, b, Li *et al*. 2008, 2018, Hou *et al*. 2018, Qiu *et al*. 2018, Qiu and Zhao 2018). However, it should be noted that the strength capacity of wire is insufficient to meet the requirement of seismic applications. Bundles of wires are needed to fulfill the strength demand of seismic dampers, and the clamping job is usually challengeable. Thus, there is a pressing need to turn the focus on the other types of SMA products, such as bars or plates.

Recently, due to the development of manufacturing technology and heating methodology of SMAs, large-size Ni-Ti SMAs have became commercially available. The potential of SMA bars can be traced back to the tensile loading tests conducted by DesRoches *et al*. (2004), in which the SMA bars exhibited desired hysteretic shape and high strength capacity. Casciati and Marzi (2010, 2011) tested the fatigue life of SMA bars. Later, Ni-Ti SMA bars were exploited in some self-centering structural components, like the beam-to-column connections in reinforced concrete frames (Youssef *et al*. 2008) or steel frames (Fang *et al*. 2017), the retrofitting elements (Shrestha *et al*. 2013, Araki *et al*. 2014), the column bases (Wang *et al*. 2019), the recentering link (Xu *et al*. 2019), and the reinforcements of bridge piers (Cruz Noguez and Saiidi 2012, Roh and Reinhorn 2010). But the dampers based on SMA bars are very limited. Almost at the meantime as this research, Wang and Zhu (2018) tested the buckling-restrained SMA bars and discussed their seismic application potential, whereas only bar is included in their work, and the effect of changing the cross section is not discussed. Besides, for this new damper which shows unsymmetrical cyclic shape, the seismic control effect under earthquake ground motions needs analysis.

To this end, this study developed an innovative self-centering damper using confined SMA cores with two different cross-sectional shapes. The considered cross sections of the SMA core include circular and rectangular shapes. Using rectangular section is inspired by the buckling-restrained brace, which is widely employed to upgrade seismic capacity for various structures in seismic prone regions and countries. Cyclic loading tests were carried out to obtain the hysteretic behavior of the damper. The characterized mechanical properties that interested by earthquake engineering include 'yielding' strength, stiffness, equivalent damping ratio and recentering capability. Due to the unsymmetrical hysteretic shape, this study further addresses the seismic control effect of the proposed damper by installing it into a multi-story frame. A conventional SMA damper in included as well for comparison purpose. The seismic analyses were conducted in the Matlab/Simulink environment. A total of twenty earthquake ground motion records was selected. In the seismic performance evaluation, interested seismic demands include the peak interstory drift, peak floor displacement, peak floor acceleration and residual displacement. Due to the special cyclic behavior possessed by the proposed damper, one additional SMA damper that represents a universal type is also analyzed for comparison purpose.

2. Design of the damper

This section introduces the design and configuration of the proposed damper. In short, the design purpose is to make full use of the tension-compression properties of SMAs. As shown in Fig. 2, the current damper consists of the following parts: (1) the SMA core, which is the main seismically-resistant component of the damper. The SMA core should be machined to dog-bone shape with the aim to concentrate deformation. The cross section of the shaped part can be circular or rectangular; (2) the confining plates, which aim to provide buckling restraint for the SMA core when the damper is subjected to compression action; (3) the bolts, which bound the confining plates and tune the distance between the SMA core and confining plates; and (4) the cellophane, which fills the gap between the SMA core and confining plates with the purpose of accommodating compression-induced poisson effect. In this design, the confining plates are also designed with high in-plane rigidity to prevent the SMA cores from being excessively compressed.

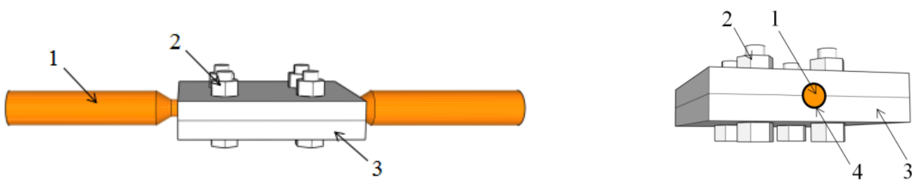

Fig. 2 Configuration of the self-centering damper using confined SMA core: 1 - SMA core; 2 - bolt; 3 -confining plate; 4 - cellophane

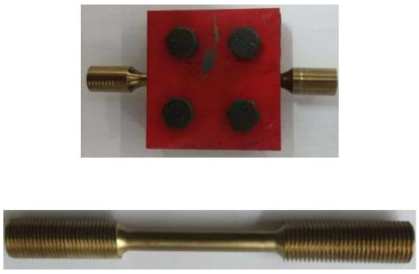

(a) SMA bar as the core

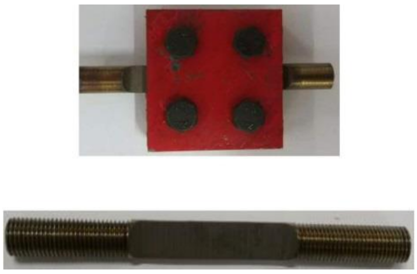

(b) SMA plate as the core

Fig. 3 Specimens of the SMA dampers

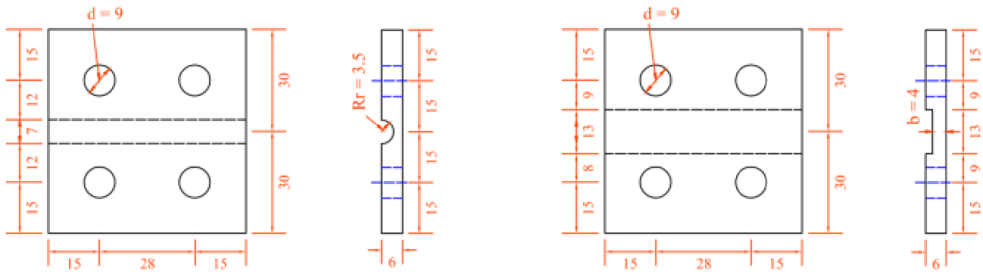

(a) Confining plates

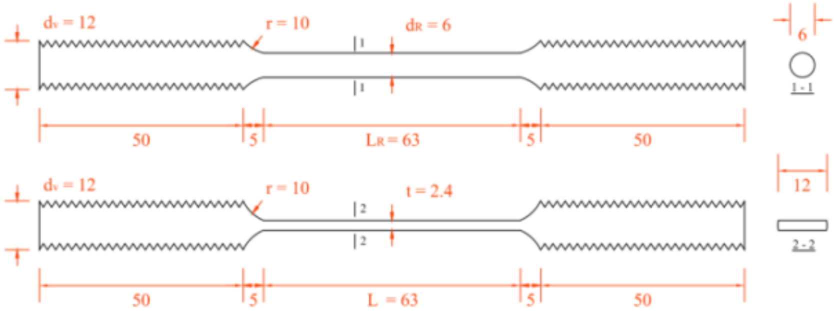

(b) SMA cores

Fig. 4 Dimensions of the dampers (unit: mm)

3. Experimental specimens and setup

The physical products and dimensions of the experimental specimens of the SMA dampers are shown in Figs. 3 and 4, respectively. The SMA cores originated from SMA raw bars. The diameter of the SMA raw bar is 12 mm with a total length of 173 mm. Both ends of the raw bar were threaded for 50 mm, which allows bolting connection. The net length of shaped part is 63 mm. To assess the effect of using different cross sections, both circular and rectangular sections were machined. The space between threaded ends and shaped part was machined with an arc of 10-mm radius, with the aims of smoothly transferring loading stress and avoiding stress concentration. During the machining process, the temperature of SMA cores were maintained by pouring water at the meantime to minimize the variation of mechanical properties caused by high temperature. The covering steel plates were designed strong with a thickness of 6 mm and a side length of 58 mm. The distance between the confining plates and the threaded ends is 5 mm to accommodate axial deformation. The cross-sectional areas of specimens S1 and S2 were designed identically thus the potential hysteresis variety is entirely attributed to the change of cross-sectional shape. To the machined part, the measured values of the cross-sectional areas are actually 28.27 and 28.61 mm^2, respectively.

As shown in Fig. 5(a), the specimens were tested on MTS universal machine. The test was a displacement-based one. Fig. 5(b) plots the time history of input displacement and the corresponding strain generated in the SMA core. As can be seen, the input loading displacement is determined to be triangular waves to model seismic actions. Each loading cycle was repeated twice to observe the property degradation phenomenon. Every single cyclic loading history lasts for 160 s, which corresponds to a loading frequency of 0.00625 Hz. The applied strain amplitude was gradually increased from 1% to 5% with an increment of 1%. The environmental temperature during the tests is real-time monitored and is found slightly oscillated around 24°C, which is higher than the austenite finish temperature limit of 0°C given by the material supplier. As suggested by prior studies (Zhu and Zhang 2007, Qiu and Zhu 2014, Wang *et al.* 2016), before formal tests, training or heating treatment is usually needed to stabilize the cyclic behavior of SMAs. Therefore, after several trials to find an appropriate scheme, this study determined a method of

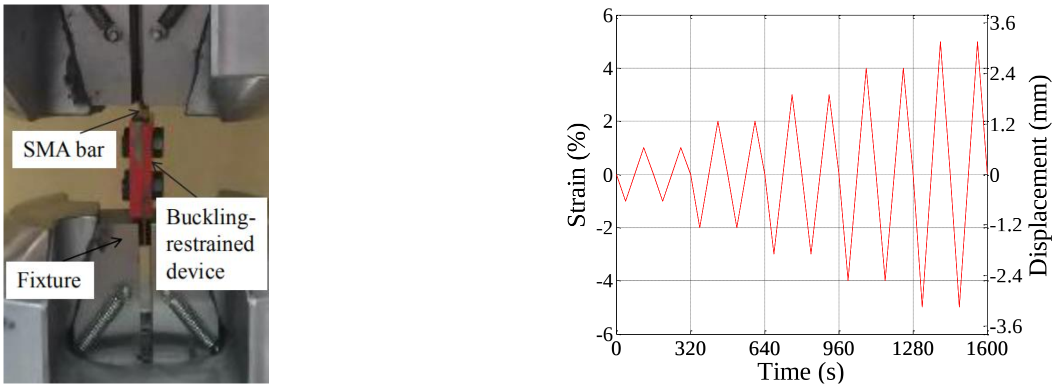

(a) Experimental setup (b) Loading scheme

Fig. 5 Experimental setup and loading scheme

initial preloading of 7% strain and then heating the specimen under 400°C for 15 minutes. The specimens were heated in Muffle furnace and cooled down in the air.

4. Test results

To quantify the cyclic behavior of the proposed damper, this section defines the parameters that of great interest in seismic applications. Fig. 6 plots the schematic of the cyclic behavior of the damper upon one single tension-compression loading cycle. The stress $\sigma = F/A$, where F and A are the force output from the MTS machine and the cross-sectional area of the SMA core, respectively; the strain $\varepsilon = \Delta L/L$, where ΔL and L are the deformation and length of the shaped part of the SMA core, since deformation is concentrated at this part. As can be seen, because of the asymmetric tension-compression behavior of the damper, the stress and strain corresponding to tension and compression actions are marked with subscripts t and c, respectively. The stresses σ_L and σ_{UL} refer to the phase transformation stress in the loading and unloading process. The strain ε_r is the residual strain when the applied stress is removed, which essentially represents the recentering capability of the damper.

Besides, to measure the nonlinear behavior of the proposed damper, three additional parameters are included:

(1) The dissipated strain energy density, E_{dis}, defined as below

$$E_{\mathrm{dis}} = \frac{W_d}{V} \tag{1}$$

where W_d is the absorbed energy in each loading cycle, which essentially equals to the enclosed area by the force-displacement curve; V is the volume of the shaped part of the SMA core.

(2) The secant stiffness, K_s, defined as below

$$K_s = \frac{(\sigma_t - \sigma_c) \times A}{(\varepsilon_t - \varepsilon_c) \times L} \tag{2}$$

where ε_t and ε_c have identical absolute values to each other, while their signs are opposite.

(3) The equivalent damping ratio, ζ_{eq}, defined as below

$$\zeta_{\mathrm{eq}} = \frac{W_d}{2\pi K_s (\varepsilon_t L)^2} \tag{3}$$

where K_s considers the effect of asymmetric cyclic behavior, accordingly, ζ_{eq} also reflects the cyclic characteristic of the damper.

Fig. 7 plots the obtained hysteretic curves of the proposed SMA damper. Desirable flag-shape hysteresis can be found in both the tension and compression actions,

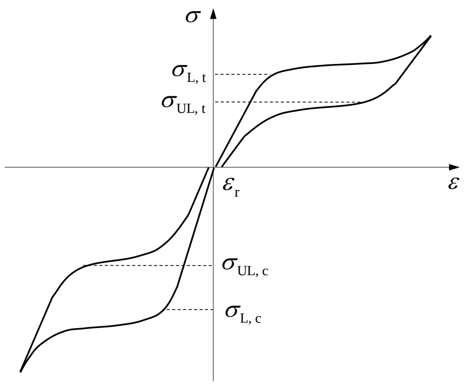

Fig. 6 Schematic of the tension-compression cyclic behavior of the SMA damper

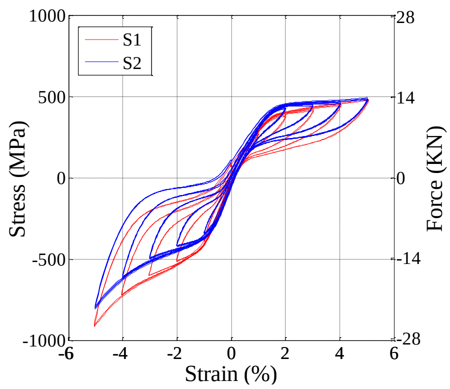

Fig. 7 Cyclic behaviors of the dampers

which successfully verifies the design purpose of making full use of the SMA material. Upon both loading directions, the hysteretic curves are featured with noticeable 'yield' point and phase transformation induced stress plateau. Primarily due to the inherent asymmetric cyclic characteristics of the SMA material, the cyclic behavior in the compression zone shows wider hysteresis, larger 'yield' strength and higher initial stiffness than that in the tension zone. The primary reason for this phenomenon is associated with the strong crystallographic texture generated in the commercial production process (Liu *et al.* 1998, Gall and Sehitoglu 1999). The hysteresis width under compression is noticeably larger than that under tension, which means the damping contrition made by the compression behavior will be higher. From this viewpoint, it is favorable to exploit the compression behavior of SMAs.

Excellent recentering capability of the damper is noticed, because the residual strain is only 0.3% even when the applied strain is up to 5%. During the total loading process, neither stiffness or strength degradation was found, because the stress generated in each cycle follows the same loading path and the second loading cycle is highly overlapped with the former one. Thus, the test results well indicate the stable hysteretic properties of the damper. When the applied strain was increased to approximately 4%, the austenite to martensite phase transformation is completed. When further deformed to 5% strain, the specimens produced slight residual strain upon complete unloading in the compression zone, because the martensite SMA generated unrecoverable crystalline dislocation. As can be foreseen, continue to load will accumulate more unrecoverable strain, the loading process is thus stopped at the 5% strain cycle to protect the damper. Besides, due to the fact that the device cannot accommodate larger loading displacement, the loading process is stopped at the 5% strain cycle. It should be noted that, although strain hardening behavior is already noticed upon 5% strain, further loading is needed to unveil the behavior at larger strain loading cycles.

The difference in the cross-sectional types of the SMA core leads to some variations in the cyclic behavior. The tested specimens S1 and S2 are comparable in the tension zone, since the corresponding behavior of the damper is entirely controlled by the tensile property of the SMA core. The strength of S2 is mildly higher than that of S1, because strength is proportional to the cross-sectional area. However, in the compression zone, these two specimens differ from each other to a certain degree, mainly in terms of strength capacity. Upon compression, S1 and S2 are identical in their initial elastic behavior, whereas S1 generates higher strength in the 'yield' stage. The underlying reason is attributed to the buckling mechanism. The compression action forced the confined SMA core into high-mode buckling behavior. In such case, because the flexural stiffness of the circular section of S1 is larger than that of the rectangular section of S2, the former exhibited higher 'yield' strength than its counterpart. For desirable dampers, the internal force generated by external loadings should be properly controlled with the aim to protect the adjacent structural members and the equivalent damping ratio should be large to inhibit and suppress vibrations. Therefore, the specimen S2, which has a flat rectangular cross section, is more favorable to seismic vibration control. This observation is consistent with the design philosophy of the widely used steel bracing damper, i.e., the buckling-restrained braces (Black *et al*. 2004).

Fig. 8 collects the interested hysteretic parameters defined in prior sections. The hysteretic properties are quantified for each complete loading cycle. In other words, both the results from tensile and compressive cycles are included. In terms of the residual strain, the larger one between those corresponding to the tensile and compressive actions is interested and presented in the figure.

According to Fig. 8(a), which presents the E_{dis} values, both dampers started to absorb energy at the strain of approximately 1% and they show almost identical trend throughout the test. In the subsequent loading cycles after the beginning of absorbing energy, the value of E_{dis} can be large to approximately 26 J/cm^3 at 5% strain. The energy dissipating mechanism is essentially associated with the recoverable phase transformations between the austenite and martensite crystalline.

Fig. 8(b) plots the relationship between the ζ_{eq} and strain amplitude. At the 1% strain cycle, the ζ_{eq} is approximately 4%, which is relatively small because the corresponding hysteresis is dominated by elastic behavior. As the strain demand is increased, the ζ_{eq} increased rapidly to over 11% at the strain cycle of 5%. The increasing rate seems saturated after the 4% strain cycle, which is affected by the suddenly increased stress when the forward phase transformation is completed. Slight difference can be found between the ζ_{eq} of these two dampers, due to the comparable e_{dis} while unequal K_s caused by different stress levels.

Fig. 8(c) shows the development of K_s during the tests. It can be seen that the initial stiffness of both dampers is approximately 15 kN/mm, since the dampers are mainly in the elastic stage at small strains. As the applied strain is increased from 1% to 2%, the dampers are deformed into the 'yield' plateau due to the austenite to martensite phase transformation of SMA cores, and the K_s drastically dropped below 10 kN/mm as a result. Further loadings continue to decrease K_s to a magnitude of approximately 6 kN/mm. Again, the lower secant stiffness of S2 is attributed to the smaller buckling-induced strength, which is beneficial to seismic applications from the perspective of well capping strength demand transferred to the adjacent structural components.

Fig. 8(d) presents the accumulation of residual deformation, D_r, during the loading process. As the applied stains are less than 4%, the values of D_r gradually increased to approximately 0.15%. Even when the applied strain is as large as 5%, the D_r suddenly doubled due to the unrecoverable martensite crystalline, but it was still only 0.3%, corresponding to 6% of the applied strain. Comparison between S1 and S2 indicates that the cross-sectional shape of the SMA cores generates minimal influence on the residual deformation. Thus, the proposed dampers are able to exhibit excellent recentering capability by using either SMA core.

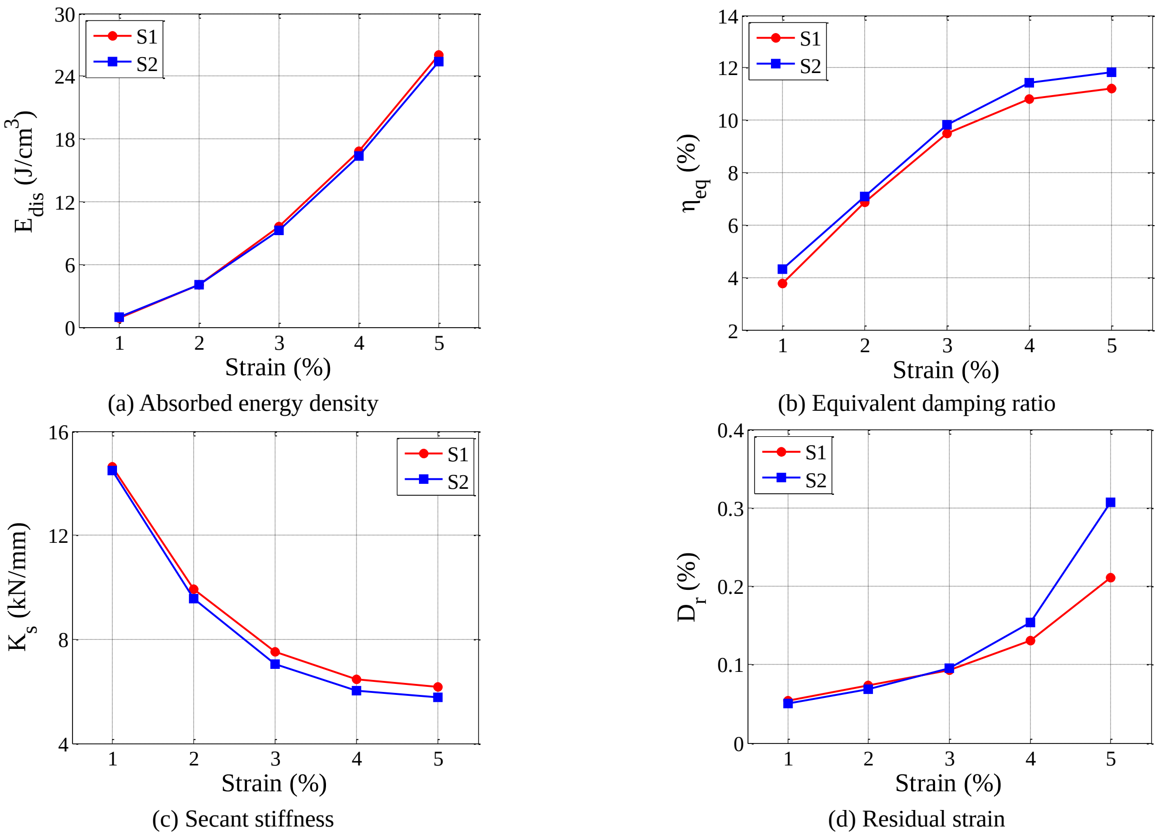

(a) Absorbed energy density
(b) Equivalent damping ratio
(c) Secant stiffness
(d) Residual strain

Fig. 8 Hysteretic properties as a function of applied strain

5. Constitutive model

Prior to conducting the seismic vibration control analysis for the proposed dampers, it is necessary to numerically simulate the test results. In earthquake engineering, the most widely accepted constitutive model for SMAs can be traced back to the work by Graesser and Cozzarelli (1991). Later, Wilde *et al.* (2000) extended this model to include the elastic behavior of martensite crystalline. Zhang and Zhu (2007) developed a modified Wilde model and applied their model to protect frame buildings. In this paper, the constitutive model proposed as below is essentially a simplified form of the Wilde model. The differential form of the stress-strain relationship is given as below

$$\dot{\sigma} = E_t\left[\dot{\varepsilon} - |\dot{\varepsilon}|\left(\frac{\sigma-\beta_t}{Y_t}\right)^{n_t}\right]u_{\mathrm{III}}(\varepsilon) + \left\{E_c\left[\dot{\varepsilon} - |\dot{\varepsilon}|\left(\frac{\sigma-\beta_c}{Y_c}\right)^{n_c}\right]u_I(\varepsilon) + (3a_1\dot{\varepsilon}\varepsilon^2 + 2a_2u(\varepsilon) + a_3\dot{\varepsilon})u_{\mathrm{II}}(\varepsilon)\right\}\left(1-u_{\mathrm{III}}(\varepsilon)\right) \tag{4}$$

$$\beta_t = E_t\alpha\left\{\varepsilon - \frac{\sigma}{E_t} + f_{Tt}|\varepsilon|^{c_t} erf(a_t\varepsilon)[u(-\varepsilon\dot{\varepsilon})]\right\} \tag{5}$$

$$\beta_c = E_c\alpha\left\{\varepsilon - \frac{\sigma}{E_c} + f_{Tc}|\varepsilon|^{c_c} erf(a_c\varepsilon)[u(-\varepsilon\dot{\varepsilon})]\right\} \tag{6}$$

$$\alpha = \frac{E_y}{E-E_y} \tag{7}$$

$$erf(x) = \frac{2}{\sqrt{\pi}}\int_0^x e^{-t^2}dt \tag{8}$$

$$u(x) = \begin{cases}1 & (x \geq 0)\\ 0 & (x < 0)\end{cases} \tag{9}$$

$$u_I(\varepsilon) = \left(1 - u_{\mathrm{II}}(\varepsilon)\right) \tag{10}$$

$$u_{\mathrm{II}}(\varepsilon) = \begin{cases}1 & (\varepsilon\dot{\varepsilon} > 0 \& \varepsilon < \varepsilon_1)\\ 0 & (\text{otherwise})\end{cases} \tag{11}$$

$$u_{\mathrm{III}}(\varepsilon) = \begin{cases}1 & (\varepsilon > 0)\\ 0 & (\text{otherwise})\end{cases} \tag{12}$$

where σ and ε are the stress and strain of SMAs; the subscripts of 't' and 'c' refer to tension and compression, respectively; E is the austenite modulus, Y is the forward phase transformation stress; n controls the sharpness of the hysteretic curves; f, a and c are parameters affecting the hysteresis shape; ε_1 is the strain corresponding to the finish of austenite to martensite phase transformation; a_1, a_2 and a_3 are related with the strain rate in martensite phase; $erf(x)$ is the error function; $u(x)$, $u_{\mathrm{I}}(\varepsilon)$, $u_{\mathrm{II}}(\varepsilon)$ and $u_{\mathrm{III}}(\varepsilon)$ are the unit-step functions.

The proposed model is examined by comparing it with test results, as shown in Fig. 9, and good agreement can be

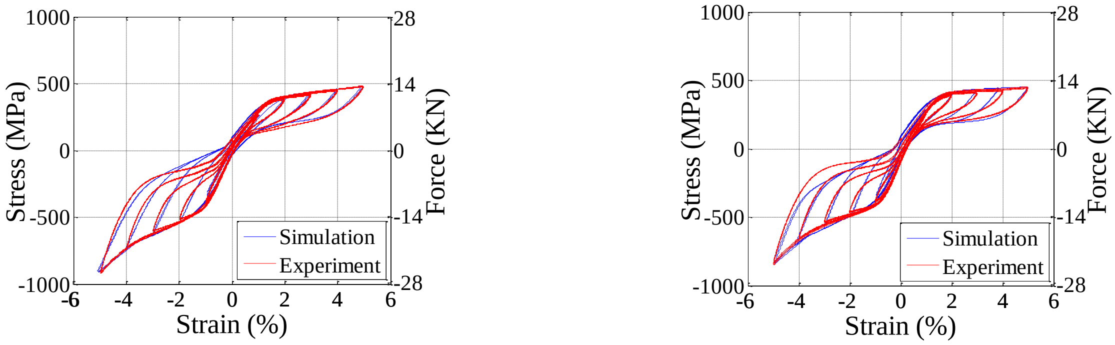

(a) S1 (b) S2

Fig. 9 Verification of the proposed constitutive model

Table 1 Calibrated parameters of the constitutive model

Damper 1 (S1)		Damper 2 (S2) *		Damper 3 *	
$\varepsilon > 0$	$\varepsilon < 0$	$\varepsilon > 0$	$\varepsilon < 0$	$\varepsilon > 0$	$\varepsilon < 0$
E_t = 24.6 GPa	E_c = 42.5 GPa	E_t = 25.9 GPa	E_c = 47.8 GPa	E_t = 25.9 GPa	E_c = 25.9 GPa
Y_t = 333 MPa	Y_c = 450 MPa	Y_t = 380 MPa	Y_c = 480 MPa	Y_t = 380 MPa	Y_c = 380MPa
α_t = 0.995	α_c = 0.241	α_t = 0.031	α_c = 0.225	α_t = 0.031	α_c = 0.031
n_t = 3	n_c = 3	n_t = 3	n_c = 3	n_t = 3	n_c = 3
f_{Tt} = 0.151	f_{Tc} = 0.056	f_{Tt} = 0.65	f_{Tc} = 0.045	f_{Tt} = 0.65	f_{Tc} = 0.65
a_t = 89	a_c = 668	a_t = 100	a_c = 500	a_t = 100	a_c = 100
c_t = 0.001	c_c = 0.001	c_t = 0.01	c_c = 0.001	c_t = 0.01	c_c = 0.01
	ε_1 = -0.037		ε_1 = -0.036		
	a_1 = 15000		a_1 = 15000		
	a_2 = 14000		a_2 = 14000		
	a_3 = 14000		a_3 = 14000		

*Note: * represents the used dampers in seismic vibration control analyses

Table 2 Comparisons between the model and test results

Specimen	Strain (%)	W_d (J)		Error (%)	K_s (kN/mm)		Error (%)	ζ_e (%)		Error (%)
		Test	Model		Test	Model		Test	Model	
S1	5	43.06	47.66	10.68	6.17	6.21	0.67	11.20	12.31	9.95
S2	5	42.54	40.00	-5.97	5.77	5.88	1.93	11.84	10.92	-7.75

found between them. Table 1 lists the calibrated parameters used in the constitutive model. Specimens S1 and S2 are denoted as Damper 1 and Damper 2, respectively. Note that the values of E and Y are directly measured from the test results; whereas the other parameters are just reasonable candidates since they do not have physical meanings. Also given in Table 1 is the parameters for Damper 3, which represents a typical SMA damper that has symmetrical behavior and will be used in the following seismic analysis. Since Damper 2 is deemed more favorable, it will be adopted in the following seismic analysis and the model parameters corresponding to tension behavior are used to describe the cyclic behavior of Damper 3. To quantify the simulation accuracy, the interested parameters associated with the 5% strain are computed and assembled in Table 2. It is seen that the errors are approximately 10%, indicating the constitutive model well captures the cyclic behavior of the damper when the hysteretic parameters are calibrated.

6. Earthquake ground motions

A total of 20 earthquake ground motion records was used in the current seismic analysis. This suite of earthquake ground motion records was originally developed for Los Angeles by Somerville *et al*. (1997). These records were derived from historical records with frequency domain adjusted and the soil type modified. The amplitudes of the ground motion records were scaled to match the design-basis earthquake seismic hazard, which represents a 10% probability of exceedence in a 50-year period. Fig. 10 plots the response spectrum of the selected ground motion records and compares the mean response spectrum with the design spectrum. Noticeable variance can be found between each single ground motion record, due to the uncertainty nature of earthquakes.

7. Building information

The 1/4-scale five-story steel frame designed by Li *et al.* (2008) was adopted as the prototype structure. This frame was also selected by Ma and Yam (2011) in their seismic vibration control analysis. As shown in Fig. 11, the frame is 1.8 m × 1.8 m in its plan layout and 4.15 m vertically. The frame is installed with inverted V-shape braces throughout building height. The seismic input direction is along with the *x* axis. The total building weight is 31.8 kN with 7.2 kN at the roof level and 6.15 kN at the other floor levels. This frame was designed by the Chinese Code for Design of Steel Structure (Chinese Standard 2003), leading to the columns using double angles 40 × 4, beams using hot-rolled steel channel 10 and braces using angle 40 × 4. Consistent with prior studies (Li *et al*. 2008, Ma and Yam 2011), the SMA damper was placed at the fist story. But it is worthwhile to evaluate the effect of varying damping locations. As the structural fuse, the SMA dampers are expected to absorb most seismic energy and concentrate inelastic deformation, and at the meantime, the main frame is protected from damage. Actually, for seismic control problems, it usually makes an assumption that the protected structure remains damage free when dampers are installed. Further, the benchmark frame is adopted from a prior study (Ma and Yam 2011), which assumes the main frame is elastic. However, it is necessary to seriously consider building nonlinearity in future. As a result, the nonlinear behavior of the damped structure is characterized by the hysteresis of SMA dampers, while the main frame stays with elastic behavior.

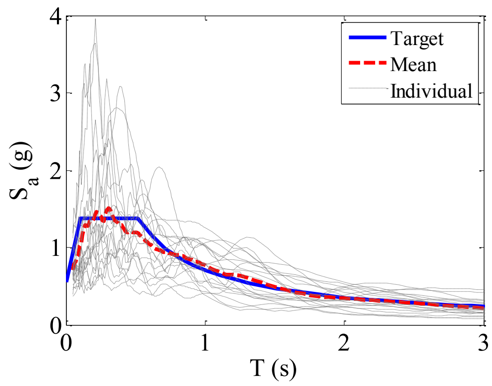

Fig. 10 Earthquake ground motion records

8. Analytical model

Belonging to a class of passive dampers, SMA dampers achieve seismic control target without requiring external power source. The working principle of using SMA dampers to control seismic response is schematically shown in Fig. 12. When the earthquake excitation is input into the main frame, the corresponding seismic response would produce deformation feedback to the SMA damper. Then

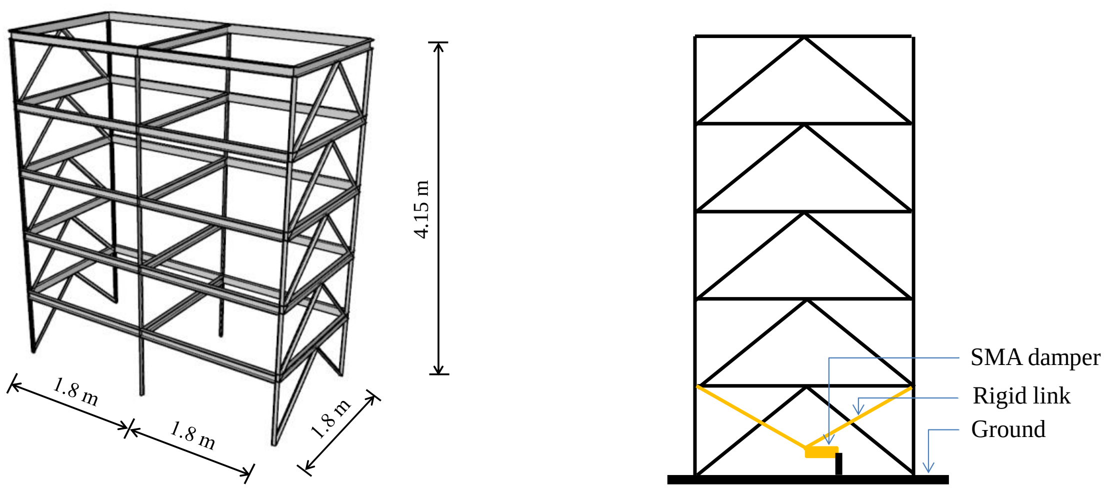

Fig. 11 Prototype frame and damper location

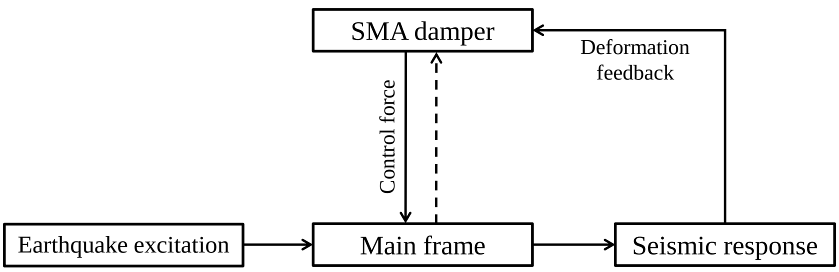

Fig. 12 Schematic of using SMA damper to control seismic response

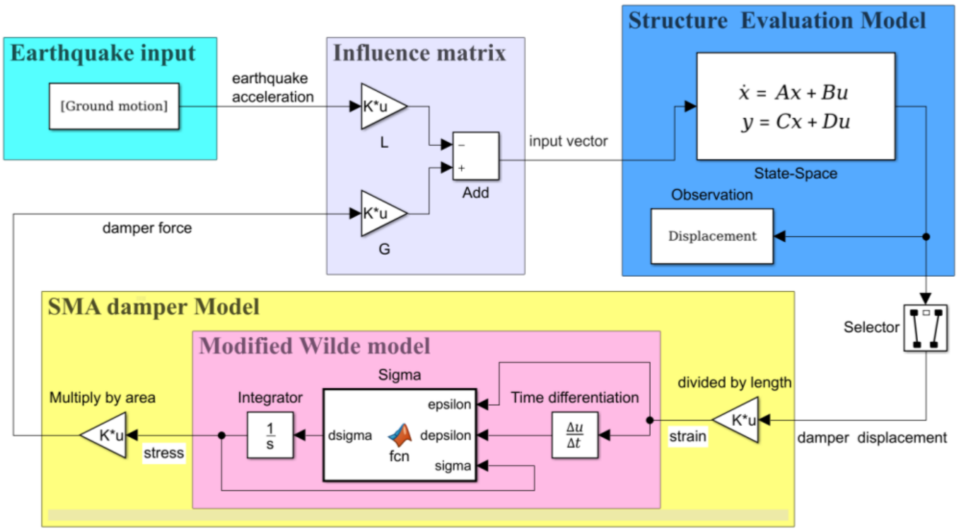

Fig. 13 Simulation in the Matlab/Simulink environment

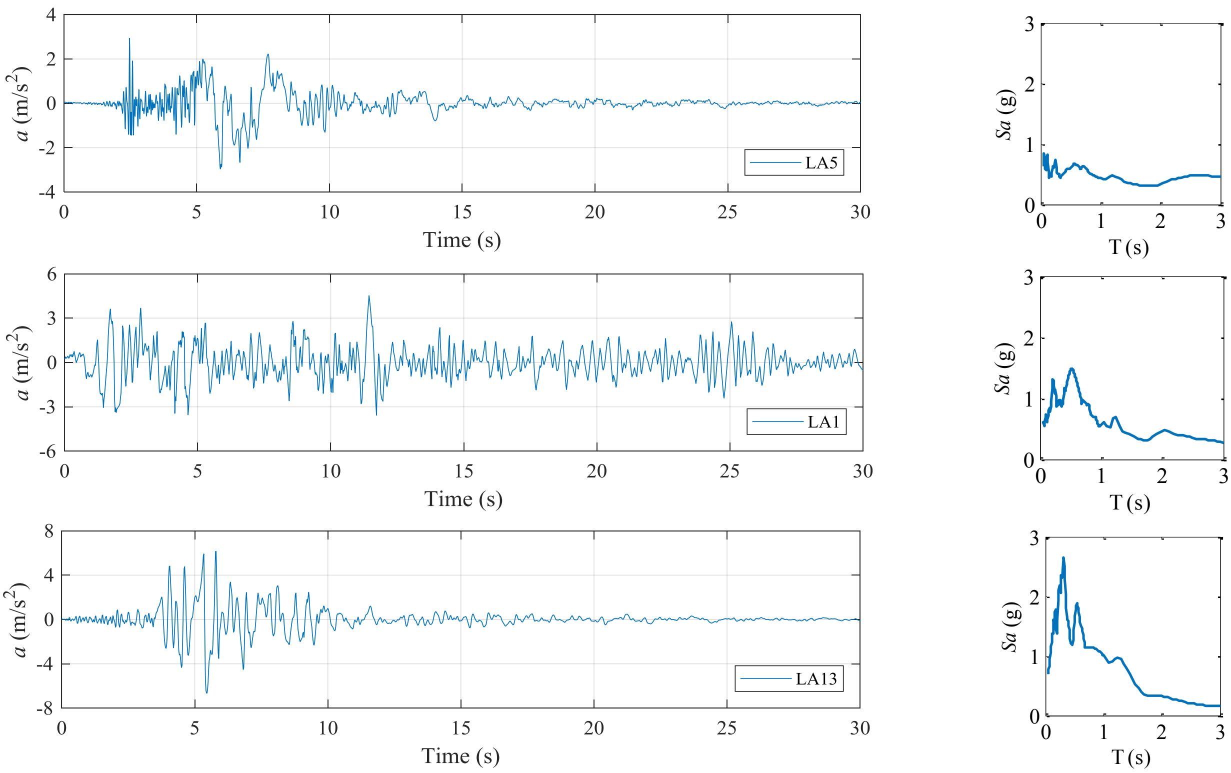

(a) Accelerogram (b) Elastic response spectrum for 5% damping

Fig. 14 Earthquake ground motion records of LA05, LA01 and LA13

the damper generates control force to the main frame and accordingly constrains structural responses. The analytical model and simulation process are programmed in the Matlab/Simulink environment, which is a powerful tool for visually addressing the dynamic problems and examining results. For single-degree-of-freedom damped systems, the equation of motion is given as below

$$m\ddot{x} + c\dot{x} + kx + \Gamma x = -m\ddot{x}_g \tag{13}$$

where m is the building mass; x is the seismic displacement relative to the ground; $\ddot{x}_g$ is ground acceleration; c is the damping coefficient; k is the lateral stiffness of the main system; Γx is the control force generated by the SMA damper; Γ is a generic integral-differential operator. In terms of the current multi-story frame, which is a multi-degree-of-freedom system, Eq. (13) should be rewritten in matrix form. The matrices of mass, stiffness and damping are taken from the study (Ma and Yam 2011). The seismic response of the damped system is simulated in the Simulink environment according to the flow chart, as shown in Fig. 13. The Eigen value analysis shows the fundamental period of the original and damped frames are 0.32 and 0.27 s, respectively.

9. Case study

Case study was conducted to have a preliminary understanding of the seismic vibration control effect of the proposed SMA damper. To this end, three representative earthquake ground motion records are artificially selected in the case study. These records include LA05, LA01 and LA13, which are supposed to represent the small, medium and large earthquakes, respectively. Fig. 14 plots the accelerogram and elastic response spectrum for 5% damping for the selected ground motions. Within the interested period range less than 1.0 s, the spectral acceleration demand of LA13 is the highest, followed by that of LA01 and LA05.

Fig. 15 firstly assesses the cyclic behavior of the SMA dampers under the selected ground motion records. The trend is clear that the nonlinear behavior of the dampers is getting increasing remarkable when the earthquake is intensified. At the small earthquake, i.e., LA05, the dampers behave in a perfectly linear fashion, as shown in Fig. 15(a). The peak displacement of Damper 2 is 0.76 mm, which is slightly smaller than the demand of Damper 3. It is also noted the higher stiffness in compression behavior of Damper 2 leads to better deformation control effect. Upon LA01, the dampers are driven into their nonlinear stage, as shown in Fig. 15(b). In this case, the nonlinear behavior is primarily activated in the tension direction. The peak displacements of Damper 2 and Damper 3 are 2.06 and 2.16 mm, respectively, showing a very close seismic deformation demands. In terms of the most intensified earthquake, LA13, the dampers exhibited strong nonlinearity in both tension and compression directions, as shown in Fig. 15(c), and they sustained similar peak deformations again. In the compression zone, it is also seen that the peak displacement of Damper 2 is smaller than that of Damper 3, due to the larger control force in the compression direction.

Response time history is plotted to demonstrate how the installed dampers affect the structural vibration mode in the time domain. Since ground motion record LA13 produced the most significant nonlinearity in both dampers, among the three selected ground motion records, the corresponding time history is plotted to highlight the response characteristics. Fig. 16 plots the response time history of displacement and acceleration at the roof level, to under the dynamic behavior in a global manner. Due to the quick decay of vibrations and to have a close-up view of the peak

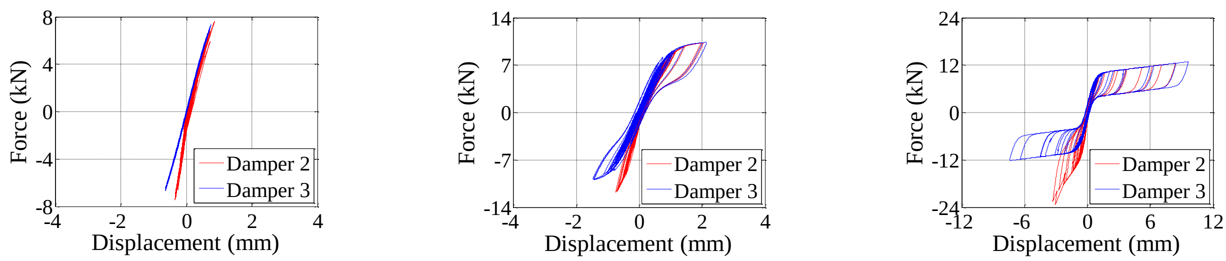

(a) LA05 (b) LA01 (c) LA13

Fig. 15 Cyclic behavior of the SMA dampers under ground motion records LA5, LA1 and LA13

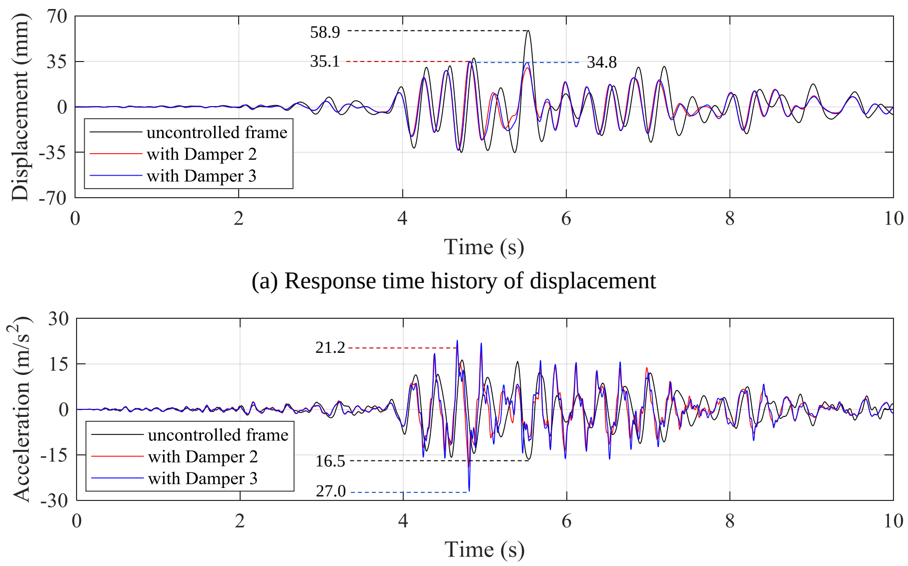

(b) Response time history of acceleration

Fig. 16 Response time history of displacement and acceleration at the roof level

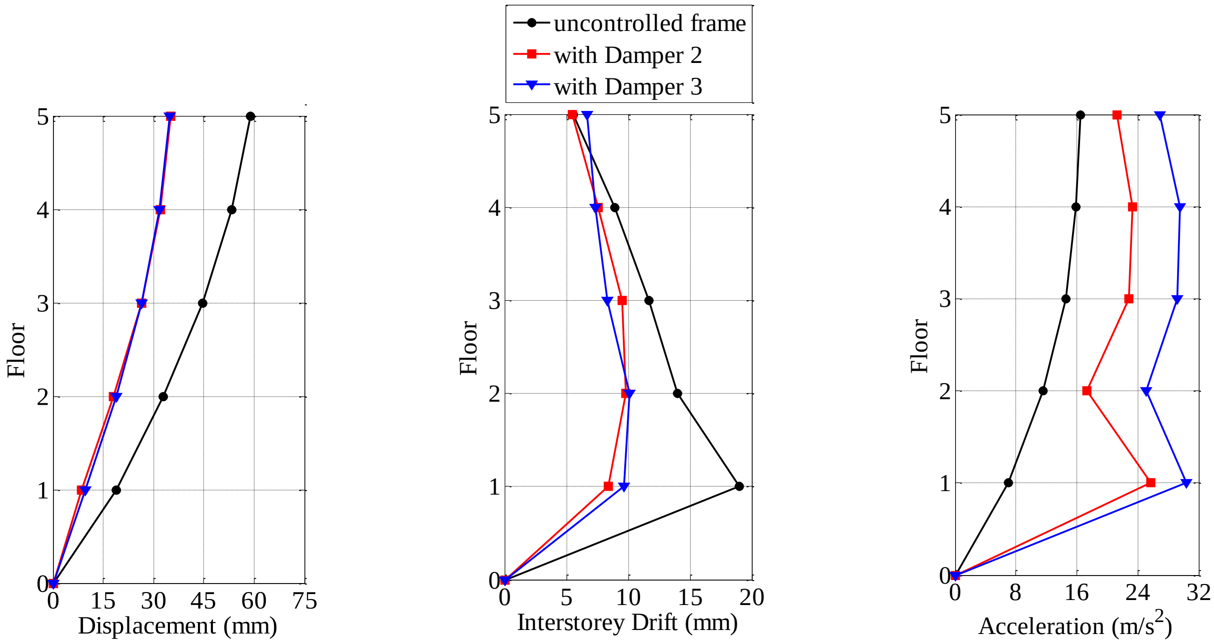

(a) Displacement (b) Interstory drift (c) Acceleration

Fig. 17 Seismic demands under LA13 along building height

demands, the response time is truncated at 10 seconds. According to this case, the roof displacement is decreased from 58.9 mm to 35.1 and 34.8 mm by Damper 2 and Damper 3, respectively, corresponding to over 40% reduction. Besides, the structures tend to vibrate around the initial position due to the self-centering capability of SMA dampers. For the acceleration demand, it is increased by both dampers which is attributed to the shortened fundamental period as dampers were installed. It is worth noting that the proposed damper leads to smaller acceleration demand than Damper 3.

Fig. 17 plots the height-wise seismic demands, including the displacements, interstory drifts and floor accelerations. The highly-overlapped curves of displacement performance demonstrate that Damper 2 achieved nearly identical deformation control effect as Damper 3. By further examining the interstory drifts, the major reduction locates at the 1st story, which takes approximately 50% in the total reduction. Combining the results of Figs. 17(a) and (b), it is found that the tension-compression asymmetry does not deteriorate the deformation control effect of SMA dampers. Regarding the floor acceleration demands, as shown in Fig. 17(c), it is interesting to note that the proposed damper exhibited smaller accelerations than the conventional SMA damper in this special case, although both dampers caused larger acceleration demands throughout building height.

10. Statistical results

Following the case study, the statistical analysis is conducted to have a more confident insight into the seismic control effect of the proposed damper over the selected suite of ground motions. The interested performance indices are the same as that focused in case study, including the maximum displacement, peak interstory drift ratio and peak floor acceleration. The residual displacement is not necessarily concerned, since the SMA dampers are inherently recentering and the main frame maintains elastic behavior. Due to the response uncertainty under different earthquakes, only the mean values of the results generated from all single cases are presented.

According to Fig. 18(a), both dampers successfully reduced the global displacement of the frame and they exhibited comparable contribution. The displacement at the first floor was reduced by 6.4 mm, which accounts for over 60% of the total displacement reduction. This indicates the displacement is mainly controlled at the first floor, i.e., the damper location. A further investigation on the displacement control can be clearly reflected by Fig. 18(b), which shows the peak interstory drift. The controlled structures show highly overlapped height-wise demands, indicating similar performance again. For the original frame, the peak interstory drift is approximately 11 mm at the first story, when the dampers are installed, the corresponding values are drastically decreased to 5.2 and 6.8 mm, respectively. But for the above stories, the reductions are getting slight when they become far away from the SMA damper. Based on the observation, it can be found that the damper mainly affects the associated story, whereas slightly alters response in the other stories.

Fig. 18(c) plots the floor accelerations along building height. After SMA dampers being installed, the lateral stiffness were increased leading to higher floor accelerations at all floor levels. In particular, the first-floor acceleration is amplified by approximately three times, due to the enhancement effect of dampers. To the other floors, their accelerations are also magnified to a certain degree by the usage of dampers. It is also worth noting that, using

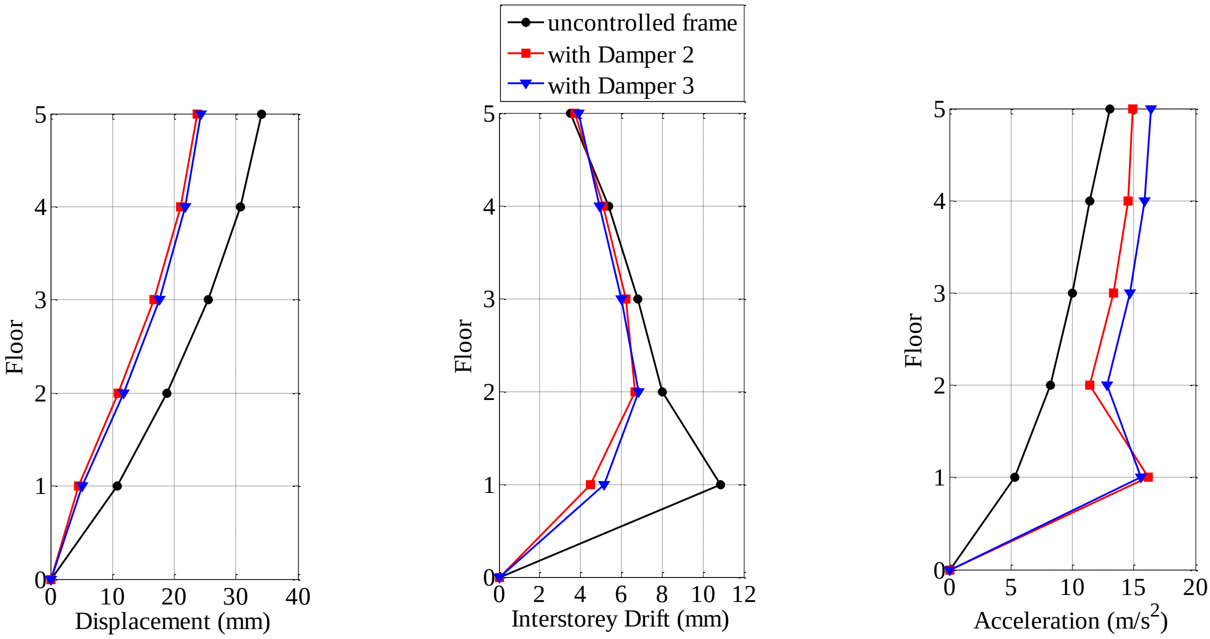

(a) Displacement (b) Interstory drift (c) Acceleration

Fig. 18 Mean seismic demands along building height under 20 ground motion records

Damper 2 tends to produce smaller accelerations than using Damper 3 in all floors except for the first floor. Therefore, the asymmetrical tension-compression behavior of SMA dampers seems beneficial to cap floor acceleration demands.

11. Conclusions

Using SMA bar or plate as the seismically-resistant core, this study proposed a buckling-restrained self-centering damper. Cyclic loading tests were conducted to verify the design concept. Further, constitutive model is proposed to simulate the hysteretic behavior of this damper and is programmed in the Matlab/Simulink environment. Both the proposed damper and conventional SMA damper are used in the seismic analysis, to assess the control efficacy of this new damper. According to the study, following conclusions can be obtained:

- Either using SMA bar or plate, the proposed dampers show desirable flag-shape hysteresis upon both tension and compression actions. From the perspective of attaining high equivalent viscous damping ratio, SMA plate is more favorable as the core of the damper.
- Upon repeated cyclic loadings, the stiffness and strength degradation were not detected. Corresponding to the maximum loading strain of 5%, the equivalent damping ratio of the SMA damper can be over 10%, implying a satisfactory damping behavior; and residual deformation is minimal, indicating excellent recentering capability.
- The proposed constitutive model successfully captures the hysteretic characteristics of the damper, and the errors of the critical hysteretic parameters between the model and test results are approximately 10%.
- According to the seismic control analysis, although the proposed damper has asymmetrical tension-compression behavior, it is able to achieve comparable seismic control target as the conventional SMA dampers. In particular, the control effect on floor accelerations was found even better by using the proposed damper. Therefore, the seismic analytical results well built confidence of using the proposed damper.

Acknowledgments

This research was supported by the National Natural Science Foundation of China (No.: 51808317) and Beijing Postdoctoral Research Foundation (No.: ZZ2019-104). However, any opinions, findings, conclusions and recommendations presented in this paper are those of the authors and do not necessarily reflect the views of the sponsors. Finally yet importantly, the authors wish to thank the anonymous reviewers for their careful evaluations and insightful comments that helped improve the paper.

References

Araki, Y., Maekawa, N., Shrestha, K.C., Yamakawa, M., Koetaka, Y., Omori, T. and Kainuma, R. (2014), "Feasibility of tension braces using Cu–Al–Mn superelastic alloy bars", *Struct. Control Health Monitor.*, **21**(10), 1304-1315. https://doi.org/10.1002/stc.1644

Bartera, F. and Giacchetti, R. (2004), "Steel dissipating braces for upgrading existing building frames", *J. Constr. Steel Res.*, **60**(3-5), 751-769. https://doi.org/10.1016/s0143-974x(03)00141-x

Bhaskararao, A.V. and Jangid, R.S. (2006), "Seismic analysis of structures connected with friction dampers", *Eng. Struct.*, **28**(5), 690-703. https://doi.org/10.1016/j.engstruct.2005.09.020

Black, C.J., Makris, N. and Aiken, I.D. (2004), "Component testing, seismic evaluation and characterization of buckling-restrained braces", *ASCE J. Struct. Eng.*, **130**(6), 880-894. https://doi.org/10.1061/(asce)0733-9445(2004)130:6(880)

Carreras, G., Casciati, F., Casciati, S., Isalgue, A., Marzi, A. and Torra, V. (2011), "Fatigue laboratory tests toward the design of SMA portico-braces", *Smart Struct. Syst., Int. J.*, **7**(1), 41-57. https://doi.org/10.12989/sss.2011.7.1.041

Casciati, S. and Marzi, A. (2010), "Experimental studies on the fatigue life of shape memory alloy bars", *Smart Struct. Syst., Int. J.*, **6**(1), 73-85. https://doi.org/10.12989/sss.2010.6.1.073

Casciati, S. and Marzi, A. (2011), "Fatigue tests on SMA bars in span control", *Eng. Struct.*, **33**(4), 1232-1239. https://doi.org/10.1016/j.engstruct.2010.12.045

Casciati, S., Faravelli, L. and Vece, M. (2017), "Investigation on the fatigue performance of Ni-Ti thin wires", *Struct. Control Health Monitor.*, **24**(1), e1855. https://doi.org/10.1002/stc.1855

Chinese Standard (2003), Code for design of steel structure GB50017, Ministry of Construction of China; Beijing, China.

Colajanni, P. and Papia, M. (1995), "Seismic response of braced frames with and without friction dampers", *Eng. Struct.*, **17**(2), 129-140. https://doi.org/10.1016/0141-0296(95)92644-n

Cruz Noguez, C.A. and Saiidi, M.S. (2012), "Performance of advanced materials during earthquake loading tests of a bridge system", *ASCE J. Struct. Eng.*, **139**(1), 144-154. https://doi.org/10.1061/(asce)st.1943-541x.0000611

DesRoches, R. and Smith, B. (2004), "Shape memory alloys in seismic resistant design and retrofit: a critical review of their potential and limitations", *J. Earthq. Eng.*, **8**(3), 415-429. https://doi.org/10.1080/13632460409350495

DesRoches, R., McCormick, J. and Delemont, M. (2004), "Cyclic properties of superelastic shape memory alloy wires and bars", *ASCE J. Struct. Eng.*, **130**(1), 38-46. https://doi.org/10.1061/(asce)0733-9445(2004)130:1(38)

Dolce, M., Cardone, D. and Marnetto, R. (2000), "Implementation and testing of passive control devices based on shape memory alloys", *Earthq. Eng. Struct. Dyn.*, **29**(7), 945-968. https://doi.org/10.1002/1096-9845(200007)29:7<945::aid-eqe958>3.3.co;2-r.

Fahnestock, L.A., Sause, R. and Ricles, J.M. (2007), "Seismic response and performance of buckling-restrained braced frames", *ASCE J. Struct. Eng.*, **133**(9), 1195-1204. https://doi.org/10.1061/(asce)0733-9445(2007)133:9(1195)

Fang, C., Wang, W., He, C. and Chen, Y. (2017), "Self-centring behaviour of steel and steel-concrete composite connections equipped with NiTi SMA bolts", *Eng. Struct.*, **150**, 390-408. https://doi.org/10.1016/j.engstruct.2017.07.067

Gall, K. and Sehitoglu, H. (1999), "The role of texture in tension–compression asymmetry in polycrystalline NiTi", *Int. J. Plastic.*, **15**(1), 69-92. https://doi.org/10.1016/s0749-6419(99)00020-0

Graesser, E.J. and Cozzarelli, F.A. (1991), "Shape-memory alloys as new materials for aseismic isolation", *ASCE J. Eng. Mech.*, **117**(11), 2590-2608. https://doi.org/10.1061/(asce)0733-9399(1991)117:11(2590)

Hou, H., Li, H., Qiu, C. and Zhang, Y. (2018), "Effect of hysteretic properties of SMAs on seismic behavior of self-centering concentrically braced frames", *Struct. Control Health Monitor.*, **25**(3), e2110. https://doi.org/10.1002/stc.2110

Katariya, P.V., Panda, S.K., Hirwani, C.K., Mehar, K. and Thakare, O. (2017), "Enhancement of thermal buckling strength of laminated sandwich composite panel structure embedded with shape memory alloy fibre", *Smart Struct. Syst., Int. J.*, **20**(5), 595-605. https://doi.org/10.12989/sss.2017.20.5.595

Li, H., Mao, C.X. and Ou, J.P. (2008), "Experimental and theoretical study on two types of shape memory alloy devices", *Earthq. Eng. Struct. Dyn.*, **37**(3), 407-426. https://doi.org/10.1002/eqe.761

Li, H.N., Huang, Z., Fu, X. and Li, G. (2018), "A re-centering deformation-amplified shape memory alloy damper for mitigating seismic response of building structures", *Struct. Control Health Monitor.*, **25**(9), e2233. https://doi.org/10.1002/stc.2233

Liu, Y., Xie, Z., Van Humbeeck, J. and Delaey, L. (1998), "A symmetry of stress-strain curves under tension and compression for NiTi shape memory alloys", *Acta Materialia*, **46**(12), 4325-4338. https://doi.org/10.1016/s1359-6454(98)00112-8

Liu, J.L., Zhu, S., Xu, Y.L. and Zhang, Y.F. (2011), "Displacement-based design approach for highway bridges with SMA isolators", *Smart Struct. Syst., Int. J.*, **8**(2), 173-190. https://doi.org/10.12989/sss.2011.8.2.173

Ma, H. and Yam, M.C. (2011), "Modelling of a self-centring damper and its application in structural control", *J. Constr. Steel Res.*, **67**(4), 656-666. https://doi.org/10.1016/j.jcsr.2010.11.014

Min, K.W., Kim, J. and Lee, S.H. (2004), "Vibration tests of 5-storey steel frame with viscoelastic dampers", *Eng. Struct.*, **26**(6), 831-839. https://doi.org/10.1016/j.engstruct.2004.02.004

Mualla, I.H. and Belev, B. (2002), "Performance of steel frames with a new friction damper device under earthquake excitation", *Eng. Struct.*, **24**(3), 365-371. https://doi.org/10.1016/s0141-0296(01)00102-x

Qiu, C. and Zhao, X. (2018), "Temperature effect on seismic performance of CBFs equipped with SMA braces", *Smart Struct. Syst., Int. J.*, **22**(5), 495-508. https://doi.org/10.12989/sss.2018.22.5.495

Qiu, C. and Zhu, S. (2014), "Characterization of cyclic properties of superelastic monocrystalline Cu-Al-Be SMA wires for seismic applications", *Constr. Build. Mater.*, **72**, 219-230. https://doi.org/10.1016/j.conbuildmat.2014.08.065

Qiu, C. and Zhu, S. (2016), "High-mode effects on seismic performance of multi-story self-centering braced steel frames", *J. Constr. Steel Res.*, **119**, 133-143. https://doi.org/10.1016/j.jcsr.2015.12.008

Qiu, C. and Zhu, S. (2017a), "Performance-based seismic design of self-centering steel frames with SMA-based braces", *Eng. Struct.*, **130**, 67-82. https://doi.org/10.1016/j.engstruct.2016.09.051

Qiu, C. and Zhu, S. (2017b), "Shake table test and numerical study of self-centering steel frame with SMA braces", *Earthq. Eng. Struct. Dyn.*, **46**(1), 117-137. https://doi.org/10.1002/eqe.2777

Qiu, C., Zhang, Y., Qi, J. and Li, H. (2018), "Seismic behavior of properly designed CBFs equipped with NiTi SMA braces", *Smart Struct. Syst., Int. J*, **21**(4), 479-491. https://doi.org/10.12989/sss.2018.21.4.479

Roh, H. and Reinhorn, A.M. (2010), "Hysteretic behavior of precast segmental bridge piers with superelastic shape memory alloy bars", *Eng. Struct.*, **32**(10), 3394-3403. https://doi.org/10.1016/j.engstruct.2010.07.013

Sabelli, R., Mahin, S. and Chang, C. (2003), "Seismic demands on steel braced frame buildings with buckling-restrained braces", *Eng. Struct.*, **25**(5), 655-666. https://doi.org/10.1016/s0141-0296(02)00175-x

Samali, B. and Kwok, K.C.S. (1995), "Use of viscoelastic dampers in reducing wind-and earthquake-induced motion of building structures", *Eng. Struct.*, **17**(9), 639-654. https://doi.org/10.1016/0141-0296(95)00034-5

Shrestha, K.C., Araki, Y., Nagae, T., Omori, T., Sutou, Y., Kainuma, R. and Ishida, K. (2013), "Effectiveness of superelastic bars for seismic rehabilitation of clay-unit masonry walls", *Earthq. Eng. Struct. Dyn.*, **42**(5), 725-741. https://doi.org/10.1002/eqe.2241

Sommerville, P., Smith, N., Punyamurthula, S. and Sun, J. (1997), "Development of ground motion time histories for Phase

2 of the FEAM/SAC steel project SAC Background document SAC", BD-91/04, SAC joint venture, Sacramento, CA, USA.
Song, G., Ma, N. and Li, H.N. (2006), "Applications of shape memory alloys in civil structures", *Eng. Struct.*, **28**(9), 1266-1274. https://doi.org/10.1016/j.engstruct.2005.12.010
Soong, T.T. and Dargush, G.F. (1997), *Passive Energy Dissipation Systems in Structural Engineering*, Wiley, New York.
Tian, L. and Qiu, C. (2018), "Controlling Residual Drift in BRBFs by Combining SCCBFs in Parallel", *ASCE J. Perform. Constr. Facil.*, **32**(4), 04018047. https://doi.org/10.1061/(asce)cf.1943-5509.0001191.
Torra, V., Carreras, G., Casciati, S. and Terriault, P. (2014), "On the NiTi wires in dampers for stayed cables", *Smart Struct. Syst., Int. J.*, **13**(13), 1738-1584. https://doi.org/10.12989/sss.2014.13.3.353
Tremblay, R., Lacerte, M. and Christopoulos, C. (2008), "Seismic response of multistory buildings with self-centering energy dissipative steel braces", *ASCE J. Struct. Eng.*, **134**(1), 108-120. https://doi.org/10.1061/(asce)0733-9445(2008)134:1(108)
Tsai, K.C., Chen, H.W., Hong, C.P. and Su, Y.F. (1993), "Design of steel triangular plate energy absorbers for seismic-resistant construction", *Earthq. Spectra*, **9**(3), 505-528. https://doi.org/10.1193/1.1585727
Wang, B. and Zhu, S. (2018), "Cyclic tension-compression behavior of superelastic shape memory alloy bars with buckling-restrained devices", *Constr. Build. Mater.*, **186**, 103-113. https://doi.org/10.1016/j.conbuildmat.2018.07.047
Wang, W., Fang, C. and Liu, J. (2016), "Large size superelastic SMA bars: heat treatment strategy, mechanical property and seismic application", *Smart Mater. Struct.*, **25**(7), 075001. https://doi.org/10.1088/0964-1726/25/7/075001
Wang, B., Zhu, S., Qiu, C. and Jin, H. (2019), "High-performance self-centering steel columns with shape memory alloy bolts: Design procedure and experimental evaluation", *Eng. Struct.*, **182**, 446-458. https://doi.org/10.1016/j.engstruct.2018.12.077
Whittaker, A.S., Bertero, V.V., Thompson, C.L. and Alonso, L.J. (1991), "Seismic testing of steel plate energy dissipation devices", *Earthq. Spectra*, **7**(4), 563-604. https://doi.org/10.1193/1.1585644
Wilde, K., Gardoni, P. and Fujino, Y. (2000), "Base isolation system with shape memory alloy device for elevated highway bridges", *Eng. Struct.*, **22**(3), 222-229. https://doi.org/10.1016/s0141-0296(98)00097-2
Xu, X., Tu, J., Cheng, G., Zheng, J. and Luo, Y. (2019), "Experimental study on self-centering link beams using post-tensioned steel-SMA composite tendons", *J. Constr. Steel Res.*, **155**, 121-128. https://doi.org/10.1016/j.jcsr.2018.12.026
Youssef, M.A., Alam, M.S. and Nehdi, M. (2008), "Experimental investigation on the seismic behavior of beam-column joints reinforced with superelastic shape memory alloys", *J. Earthq. Eng.*, **12**(7), 1205-1222. https://doi.org/10.1080/13632460802003082
Zhang, Y. and Zhu, S. (2007), "Shape memory alloy-based reusable hysteretic damper for seismic hazard mitigation", *Smart Mater. Struct.*, **16**, 1603-1613. https://doi.org/10.1088/0964-1726/16/5/014
Zhang, Y. and Zhu, S. (2008), "Seismic response control of building structures with superelastic shape memory alloy wire dampers", *ASCE J. Eng. Mech.*, **134**(3), 240-251. https://doi.org/10.1061/(asce)0733-9399(2008)134:3(240)
Zhu, S. and Zhang, Y. (2007), "Seismic behaviour of self-centring braced frame buildings with reusable hysteretic damping brace", *Earthq. Eng. Struct. Dyn.*, **36**(10), 1329-1346. https://doi.org/10.1002/eqe.683

FS